

## Effect of Polycaprolactone Scaffold Permeability on Bone Regeneration *In Vivo*

Anna G. Mitsak, M.S.,<sup>1</sup> Jessica M. Kemppainen, Ph.D.,<sup>1</sup> Matthew T. Harris, M.S.,<sup>1</sup> and Scott J. Hollister, Ph.D.<sup>1-3</sup>

Successful bone tissue engineering depends on the scaffold's ability to allow nutrient diffusion to and waste removal from the regeneration site, as well as provide an appropriate mechanical environment. Since bone is highly vascularized, scaffolds that provide greater mass transport may support increased bone regeneration. Permeability encompasses the salient features of three-dimensional porous scaffold architecture effects on scaffold mass transport. We hypothesized that higher permeability scaffolds will enhance bone regeneration for a given cell seeding density. We manufactured poly- $\epsilon$ -caprolactone scaffolds, designed to have the same internal pore design and either a low permeability ( $0.688 \times 10^{-7} \text{m}^4/\text{N}\cdot\text{s}$ ) or a high permeability ( $3.991 \times 10^{-7} \text{m}^4/\text{N}\cdot\text{s}$ ), respectively. Scaffolds were seeded with bone morphogenic protein-7-transduced human gingival fibroblasts and implanted subcutaneously in immune-compromised mice for 4 and 8 weeks. Micro-CT evaluation showed better bone penetration into high permeability scaffolds, with blood vessel infiltration visible at 4 weeks. Compression testing showed that scaffold design had more influence on elastic modulus than time point did and that bone tissue infiltration increased the mechanical properties of the high permeability scaffolds at 8 weeks. These results suggest that for polycaprolactone, a more permeable scaffold with regular architecture is best for *in vivo* bone regeneration. This finding is an important step toward the end goal of optimizing a scaffold for bone tissue engineering.

### Introduction

**B**IOMATERIAL SCAFFOLDS DELIVERING osteogenic factors are a potential alternative to traditional repair techniques for challenging clinical bone defects resulting from trauma, tumor resection, and developmental anomalies. Defining the optimal scaffold for these purposes requires determination of key parameters that have the greatest influence on bone regeneration. For defects of clinically relevant size and shape, the scaffold should allow sufficient nutrient diffusion and waste removal while simultaneously providing adequate load bearing capabilities. Generally speaking, there is a trade-off between these two requirements, as scaffold architectures designed to maximize nutrient diffusion typically result in decreased scaffold mechanical strength. Optimization of scaffold design to satisfy both of these constraints remains a challenge. Therefore, it is important to understand the impact that each of these putative design requirements have on bone regeneration.

Porosity, pore size, and permeability are interrelated architectural properties that have been shown to influence both diffusion and scaffold mechanical properties.<sup>1,2</sup> Unlike porosity, pore size, and a number of other structural parameters that have been studied, permeability defines the physical

property of mass transport, which inherently describes the effects that these structural design properties have on fluid transport into and out of a construct. The effects that scaffold permeability has on bone tissue regeneration have not been studied in depth using rigorously controlled porous architectures with reproducibly designed effective permeability. In this work, scaffolds are designed such that permeability changes, whereas pore shape, pore size, and pore interconnectivity are held constant between groups to specifically compare the effects of increasing permeability on bone growth. Image-based design combined with solid free form fabrication (SFF) enables the creation of scaffolds that have precise permeability characteristics resulting from rigorously controlled three-dimensional (3D) architecture. By using these techniques, the effects that permeability has on the growth of bone tissue into a scaffold can be investigated, providing important considerations for developing optimized constructs.

In recent literature, the range of variables examined for their effect on bone growth extends beyond scaffold design to include cell type, growth factors, and scaffold material. Common cell types studied for bone regeneration include fibroblasts, osteoblasts, and stem cells, often combined with one or more growth factors such as insulin-like growth

Departments of <sup>1</sup>Biomedical Engineering, <sup>2</sup>Mechanical Engineering, and <sup>3</sup>Surgery, University of Michigan, Ann Arbor, Michigan.

factor, transforming growth factor beta, or bone morphogenic proteins (BMP). These cells and growth factors are housed within scaffolds made of a variety of materials. Polypropylene fumarate,<sup>3,4</sup> poly-ε-caprolactone (PCL),<sup>5-7</sup> polylactic acid,<sup>8,9</sup> and poly(lactic-co-glycolic) acid<sup>10,11</sup> are bioresorbable polymers that have all been investigated, alone or in combination, for bone applications, as have osteoconductive materials such as tricalcium phosphate,<sup>8</sup> hydroxyl apatite,<sup>12</sup> and calcium phosphate.<sup>13,14</sup>

This work employs the use of PCL scaffolds seeded with BMP-7-transduced human gingival fibroblasts to study the effects that permeability has on bone tissue regeneration. PCL has been used extensively for tissue engineering applications.<sup>5-7,15,16</sup> The degradation profile and mechanical properties of this polymer support its use for bone tissue engineering. In terms of manufacturability, the polymer is favorable both for studying scaffold architecture effects on tissue regeneration and for subsequent clinical tissue engineering applications, as PCL scaffolds can be created using many SFF techniques. These include selective laser sintering,<sup>6</sup> fused deposition modeling,<sup>15</sup> photopolymerization of PCL macromer,<sup>16</sup> and 3D printing.<sup>7</sup> Specifically for the purposes of this study, PCL is compatible with the image-based design and 3D printing-direct casting techniques we have used to fabricate consistent, reproducible scaffolds with designed architectures. BMP-7-transduced fibroblasts were utilized as a cell source known to reproducibly generate bone in ectopic sites.<sup>7,17</sup> Various studies have investigated scaffold architectures that may or may not affect bone growth, with many hypothesizing that results are dependent on the fluid flow and nutrient/waste diffusion properties imposed by the design parameters utilized.<sup>1,2,16</sup> Roosa *et al.*<sup>7</sup> determined that different pore sizes (350, 500, and 800 μm) had little effect on *in vivo* bone growth using PCL scaffolds. Others have concluded that increased scaffold porosity is important for cell delivery<sup>18</sup> and sufficient diffusion of nutrients and waste into and out of the scaffold. While studies may support or refute the requirement of specific pore sizes and shapes, strut/fiber diameters, interconnectivity, or porosities individually for optimal bone growth, it is important to acknowledge that these design parameters (1) are related to and contingent on one another, and (2) may have a profound effect on the mechanical properties of scaffolds. This work primarily addresses the first challenge by proposing a more definitive way to examine impacts that scaffold architectures may have on tissue growth. This is done by studying the effects of scaffold permeability, a design parameter that, in terms of fluid flow, incorporates all of these design variables.

This work also addresses the second concern of maintaining sufficient mechanical properties to support developing tissue while optimizing scaffold architecture for enhanced bone regeneration. By inference, if permeability is shown to affect the amount of bone generated on PCL scaf-

folds, structural parameters such as pore size and shape, interconnectivity, strut size and shape, and porosity can be manipulated to meet biomechanical requirements, whereas permeability requisites are also maintained within desired ranges. Alternatively, if permeability is shown to have no effect on bone regeneration, these structural parameters can be optimized strictly for mechanical or other desired properties. Further, the work determines the mechanical properties of the scaffold architectures used and compares their modulus and strength to that of native bone as a proof of concept for using PCL to fabricate scaffolds for bone tissue applications.

This study specifically addresses the importance of scaffold permeability as a design parameter and the need for balancing pore geometry with mechanical properties to create scaffolds that allow for bone regeneration and support load, and can be easily manufactured. By utilizing two scaffold designs that held pore shape, pore size, and pore interconnectivity constant yet resulted in differing permeability, the effect that the latter parameter has on bone regeneration was evaluated in terms of (1) volume, mineral density, and mineral content of bone within the entire scaffold, assessed by micro-computed tomography (μCT) and histology, (2) penetration of bone through the interior of the scaffold, assessed by μCT analysis with concentric regions of interest [ROI], and (3) compressive modulus and strength of resultant bone-polymer constructs, assessed by unconfined compression testing for 4 and 8 weeks in a previously characterized immune-compromised mouse model.<sup>7,17,19</sup>

## Materials and Methods



### Scaffold fabrication

Low and high permeability scaffolds were previously designed to have a permeability of 0.688 or 3.991 ( $\times 10^{-7} \text{ m}^4/\text{N-s}$ ), respectively.<sup>20</sup> The low and high permeability designs have porosities of 53.46% and 70%, and surface areas of 317.69 and 260.52 mm<sup>2</sup>, respectively. The designs and associated properties are displayed in Table 1. Inverse wax molds were built on a Solidscape Model Maker II machine (Solidscape, Merrimack, NH) and subsequently melt cast into PCL powder (43–50 kDa; Polysciences, Warrington, PA) at 115°C. The cast scaffolds were cooled and hardened overnight in a Teflon mold, placed in 100% ethanol to dissolve the wax mold, trimmed, and cleaned with wire. Before cell seeding, the scaffolds were sterilized by placing them in 70% ethanol for 24 h, followed by sterile water for 24 h and serum-free medium overnight.

### Cell culture and subcutaneous implantation procedure

Human gingival fibroblasts (ScienCell Research Laboratories, Carlsbad, CA) were cultured in Dulbecco's modified

TABLE 1. SCAFFOLD DESIGN PARAMETERS

|   |                   | Permeability<br>( $\times 10^{-7} \text{ m}^4/\text{N-s}$ ) | Porosity<br>(%) | Surface<br>area (mm <sup>2</sup> ) | Pore<br>shape | Pore<br>size (mm) | Pore<br>interconnectivity (%) |
|---|-------------------|---|-----------------|------------------------------------|---------------|-------------------|-------------------------------|
|  | Low permeability  | 0.688   | 53.46           | 317.69                             | Sphere        | 1.0               | 100                           |
|  | High permeability | 3.991   | 70              | 260.52                             | Sphere        | 1.0               | 100                           |

Eagle's medium, supplemented with 10% fetal calf serum and 5% penicillin/streptomycin (all reagents from Gibco, Carlsbad, CA). Four-week and 8-week studies were carried out separately. For each study, cells were cultured until a sufficient number of cells were reached. The day before implantation, the cells were transduced with Ad-BMP-7 (Vector Core, University of Michigan, Ann Arbor, MI) at a concentration of 500 plaque forming units per cell. On the day of implantation,  $0.75 \times 10^6$  cells were seeded into each scaffold (6.35 mm diameter, 3 mm height) using a 1:20 thrombin:fibrinogen gel for cell encapsulation. Previous studies have confirmed even seeding of cells throughout the scaffolds using this technique. Seeded scaffolds ( $n=18$  per low and high permeability design, for each time point) were kept on ice before subcutaneous implantation in the backs of NIH5-bg-nu-xid mice (Harlan Laboratories, Indianapolis, IN). Scaffolds infiltrated with a 1:20 thrombin/fibrinogen gel alone (no cells) were used as controls. After 4 or 8 weeks, mice were euthanized and scaffolds were removed, and then placed in Z-Fix overnight, in water for 2 h and stored in 70% ethanol. Fourteen specimens were excluded from analysis (2 low permeability/4 weeks, 7 low permeability/8 weeks, and 5 low permeability/8 weeks) due to the death of three animals and difficulties encountered in scaffold processing. This study was conducted in accordance with the regulations set forth by the University Committee on Use and Care of Animals at the University of Michigan.

#### $\mu$ CT analysis

Explanted, fixed scaffolds were scanned in water with a high-resolution  $\mu$ CT scanner (GE Medical Systems, Toronto, Canada) at 75 kV and 75 mA. Bone volume (BV) was analyzed using GEMS Microview software (GE Medical Systems) to obtain BV, tissue mineral density (TMD), and tissue mineral content (TMC) data, using a bone threshold value of 1100. TMD measures the degree of mineralization of tissue that has been designated bone by the  $\mu$ CT threshold analysis value (1100) within a given volume, and has units of mass of hydroxyapatite per volume (mg HyAp/mL). TMC quantifies the amount of mineralized tissue in the given ROI and has units of mass of hydroxyapatite (mg HyAp). A cubic ROI exceeding scaffold boundaries was used for "total bone volume" values (includes bone grown inside and outside scaffold boundaries). To assess the bone grown within the entire scaffold, a cylindrical ROI with fixed x and y-dimensions of 6.3455 mm and an average z-dimension of  $2.5786 \pm 0.3963$  was used. The total volume of bone generated within scaffold boundaries ("scaffold bone volume"), the percentage of available pore space occupied by bone ("bone in-growth"), TMD, and TMC were calculated. Pore volume fractions of 0.574 and 0.738 (for the low and high permeability designs, respectively) were multiplied by bounding scaffold dimensions to calculate available pore volume.

To assess the amount and quality of bone grown at various radial distances into the scaffold,  $\mu$ CT analysis was performed on each specimen using four concentric, hollow, cylindrical ROIs, with the same "z" dimensions as the entire scaffold ROIs and having outer diameters of 6.35, 5.06, 3.81, and 2.54 mm. Each of the four ROIs had inner diameters of 5.06, 3.81, 2.54, and 0.00 mm, respectively. BV, bone in-growth, TMD, and TMC were calculated for each ROI.

#### Unconfined compression testing

Explanted, fixed experimental and control scaffolds were mechanically tested in unconfined compression using an MTS Alliance RT30 electromechanical test frame (MTS Systems Corp., Minneapolis, MN). Specimens were compressed to 40% strain between two fixed steel platens at a rate of 1.0 mm/min after a 0.5 lbf preload was applied. Data were collected and analyzed using TestWorks4 software (MTS Systems Corp.). Compressive modulus was defined as the slope of the tangent line to the stress-strain curve at 12.5% strain. Compressive yield strength was calculated as the load carried at the 0.2% offset point divided by the original scaffold cross-sectional area.

#### Histology

At each time point, two fixed scaffolds from each group were sectioned and stained with hematoxylin and eosin to observe tissue morphology. Sections were viewed under a light microscope and images were obtained at 50 $\times$ , 100 $\times$ , 200 $\times$ , and 400 $\times$  magnification.

#### Statistics

Multiple linear regression, performed using SPSS software (SPSS for Windows, Rel 14.0. 2005; SPSS, Inc., Chicago, IL), was used to determine which factors (scaffold design or time) had a significant effect on a given response variable.

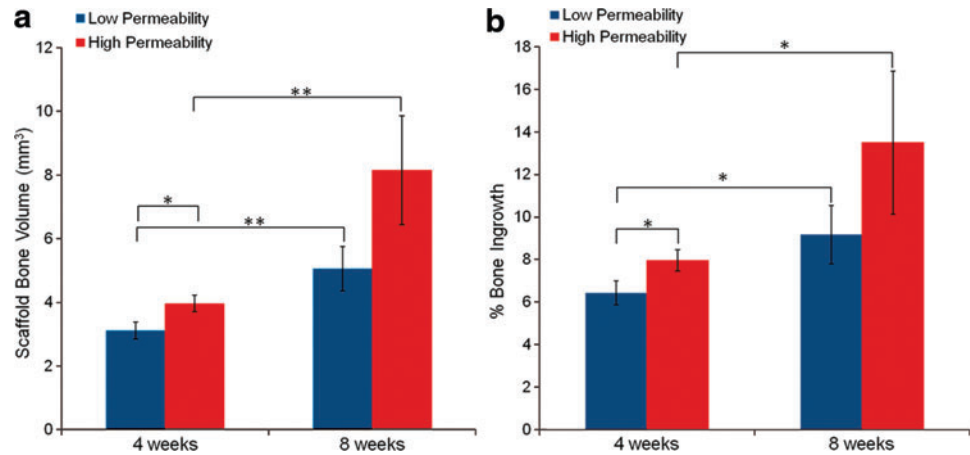
## Results

### Micro-CT

**Entire scaffold analysis.**  $\mu$ CT analysis demonstrated that total BV (scaffold BV plus bone surrounding the scaffold) did not differ between the low and high permeability scaffold designs at either time point. However, scaffold BV did differ between designs (see Fig. 1a). Scaffold BV was significantly greater for the high permeability design ( $p \leq 0.05$ ) as compared to the low permeability design at 4 weeks and was also greater for the high permeability design at 8 weeks, although this difference was not significant ( $p = 0.11$ ). Both designs demonstrated a statistically significant increase in scaffold BV at 8 weeks as compared to 4 weeks ( $p \leq 0.01$ ). Bone in-growth (Fig. 1b) significantly increased with time ( $p \leq 0.05$ ) for both designs. Also, the high permeability design showed greater bone in-growth as compared to the low permeability design at 4 weeks ( $p \leq 0.05$ ). At 8 weeks, the high permeability scaffolds again averaged a higher bone in-growth than low permeability scaffolds, but this difference was not significant ( $p = 0.25$ ).  $\mu$ CT slices through the middle of a high and a low permeability scaffold after 8 weeks *in vivo* (Fig. 2b, d) show that there appears to be more mineralized tissue in the center of the high permeability scaffolds, compared to the low permeability scaffolds. The concentric cylinder analysis further demonstrated this phenomenon (see below).

TMC values within the scaffold space for 4 and 8 weeks are displayed in Figure 3a. Time had a greater influence on TMC than scaffold design did, with significant increases in TMC from 4 to 8 weeks for both scaffold designs ( $p \leq 0.05$ ). TMC was also greater for high permeability scaffolds compared to low permeability scaffolds at 4 weeks ( $p \leq 0.05$ ).

**FIG. 1.** (a) Bone volume (BV) inside the scaffold ROI at 4 and 8 weeks. (b) Bone in-growth for the entire scaffold ROI at 4 and 8 weeks. \* $p \leq 0.05$ . \*\* $p \leq 0.01$ . ROI, region of interest. Color images available online at [www.liebertonline.com/tea](http://www.liebertonline.com/tea)

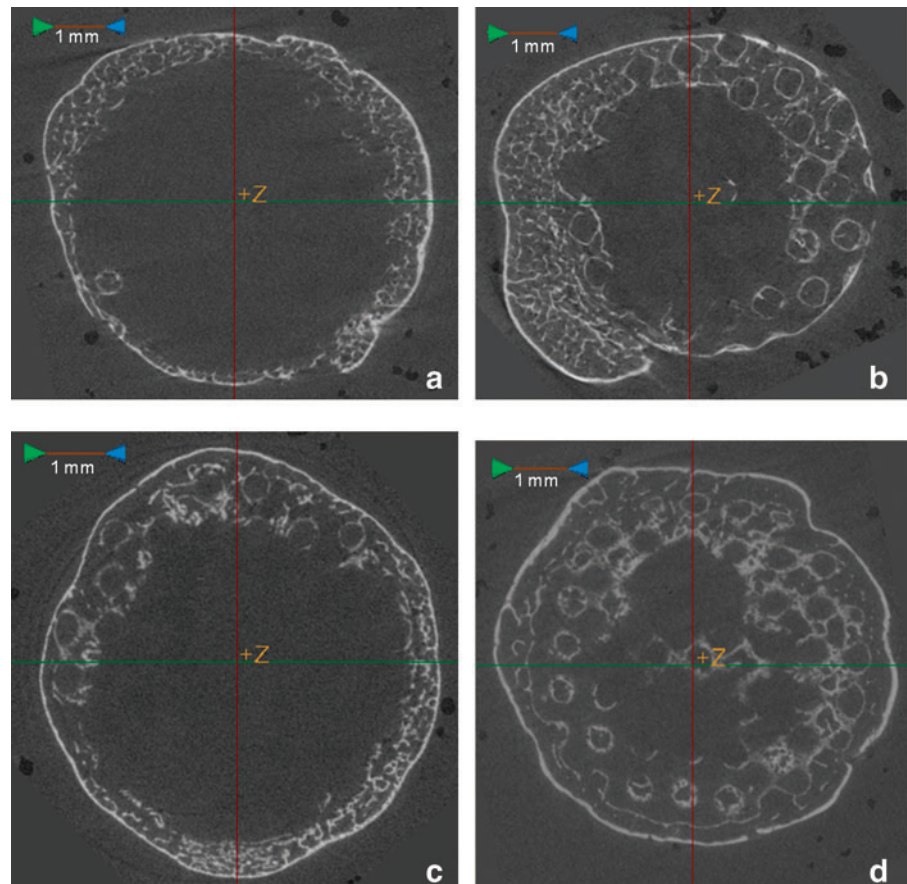


Average TMD values for bone grown on each design at both 4 and 8 weeks (range = 360–600 mg/mL) fell within the ranges of normal human trabecular and cortical bone<sup>21</sup> and are displayed in Figure 3b. Time *in vivo* had a greater influence on TMD values than scaffold design did. No significant differences in TMD were seen between scaffold design at either time point, but TMD increased significantly from 4 to 8 weeks for both scaffold designs ( $p \leq 0.05$ ).

**Concentric cylinder analysis.** The diameters of the cylindrical ROIs were decreased by 1.29 mm each time to create a set of four, concentric ROIs, as shown in Figure 4. For each

of these regions, the high permeability scaffolds at 8 weeks contained more BV than their low permeability counterparts, with significant differences ( $p \leq 0.01$ ) for ROI 2, ROI 3, and ROI 4 (ROI 1 did not show significance at a 0.05 level, although the  $p$ -value was still relatively low, at  $p = 0.1$ ), as shown in Figure 5a. This shows that bone penetrated into the center of the scaffold and was not confined to the edges of the scaffold. For bone in-growth, the most interesting comparisons were those between ROIs for each scaffold design group, as shown in Figure 5b. For both scaffold designs at 4 weeks and for the low permeability design at 8 weeks, in-growth significantly decreased going from the entire scaffold

**FIG. 2.** Micro-CT image slices from the center of representative low and high permeability scaffolds. (a) Low permeability scaffold at 4 weeks, (b) low permeability scaffold at 8 weeks, (c) high permeability scaffold at 4 weeks, and (d) high permeability scaffold at 8 weeks. Color images available online at [www.liebertonline.com/tea](http://www.liebertonline.com/tea)



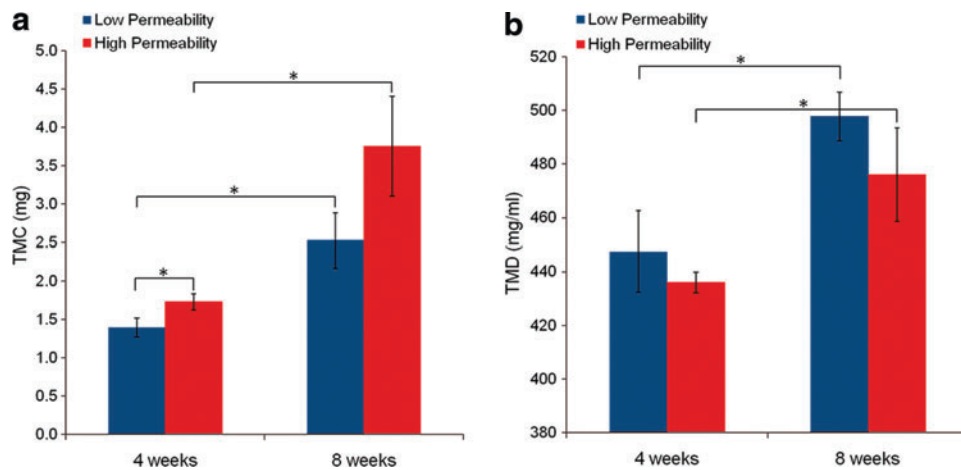


**FIG. 3.** (a) Tissue mineral content (TMC) and (b) tissue mineral density (TMD) at 4 and 8 weeks. \* $p \leq 0.05$ . Color images available online at [www.liebertonline.com/tea](http://www.liebertonline.com/tea)

ROI to smaller ROIs. This would suggest that for these groups, in-growth is not maintained throughout the scaffold. However, for the high permeability scaffolds at 8 weeks, this decrease is not observed, demonstrating that in-growth of bone is seen throughout the entire scaffold progressing through to the center of the scaffold.

#### Compression testing

Tangent modulus at 12.5% strain and compressive yield strength at the 0.2% offset yield point are shown in Figure 6 for both scaffold designs and both time points. Modulus and compressive yield strength values of low permeability scaffolds were significantly higher than those for high permeability scaffolds at 0, 4, and 8 weeks ( $p \leq 0.01$ ). Time *in vivo* did not significantly affect tangent modulus values of scaffold–bone constructs for the low permeability design. However, for the high permeability design, there is a significant

increase ( $p \leq 0.01$ ) in modulus at 8 weeks. Similarly, compressive yield strength (Fig. 6b) increases significantly ( $p \leq 0.05$ ) from 0 to 4 and from 4 to 8 weeks for the high permeability design. Average yield strength of low permeability constructs also increased between zero and 4 weeks ( $p \leq 0.01$ ), but a decrease was seen between 4 and 8 weeks ( $p \leq 0.01$ ).

#### Histology

Histological analysis confirmed bone growth (reported quantitatively through  $\mu$ CT assessment) in and around scaffold pores. Figure 7 shows representative histological sections from an 8-week, high permeability scaffold at 50 $\times$  and 400 $\times$  (panels a and b, respectively), and an 8-week, low permeability scaffold at 50 $\times$  and 400 $\times$  (panels c and d, respectively). In the low magnification images, the dark pink staining representing bone is indicated by the arrows and is

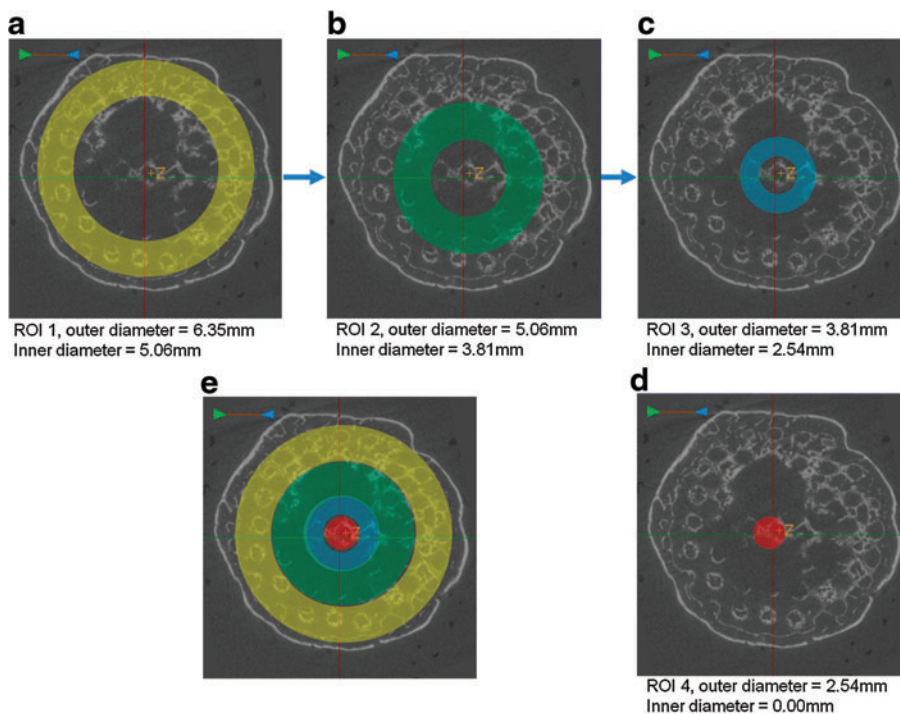


**FIG. 4.** Micro-CT slice images showing top-down views of the cylindrical ROIs used for the concentric BV analysis. (a–d) show the four concentric ROIs, each with a progressively smaller outer diameter, and (e) shows all four ROIs overlaid on one another. Color images available online at [www.liebertonline.com/tea](http://www.liebertonline.com/tea)

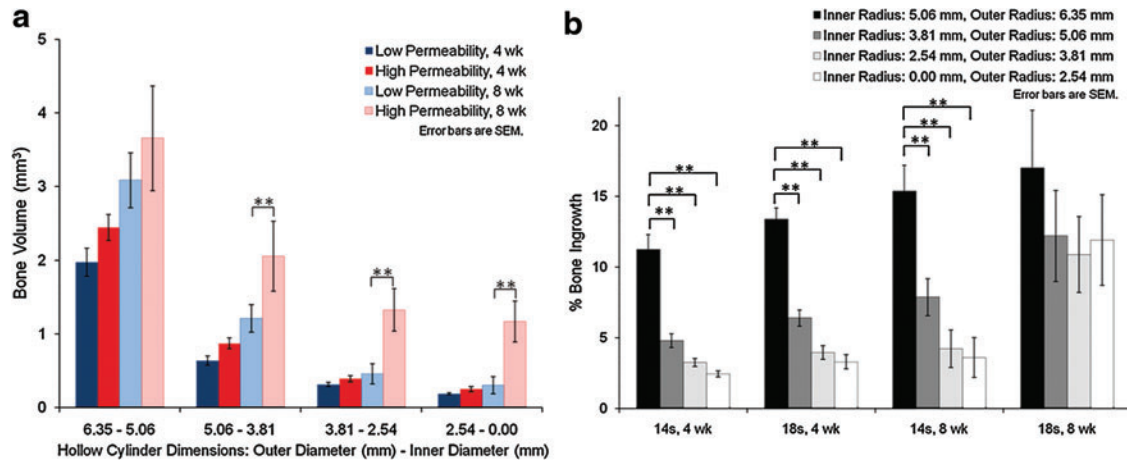


**FIG. 5.** Concentric cylinder BV analysis. (a) BV and (b) bone in-growth for high and low permeability scaffolds and 4 and 8 weeks, for four hollow, cylindrical ROIs.  $**p \leq 0.01$ . Color images available online at [www.liebertonline.com/tea](http://www.liebertonline.com/tea)

visible in the pore spaces of the representative high permeability scaffold (a). For the low permeability scaffold (c), this dark pink staining is mainly seen toward the outer edges of the construct. Marrow space is indicated in the images by the letter "M," osteocytes in lacunae are circled, and blood vessel infiltration is indicated by "BV." All scaffolds displayed a thin layer of bone around the outside of the scaffold. Compared to lower permeability scaffolds, the higher permeability scaffolds showed more evidence of bone spicules growing within the pore space, as shown by greater areas of dark pink staining.

## Discussion

The ultimate goal of utilizing biomaterial scaffolds for bone tissue engineering applications is to develop constructs that support or even enhance bone regeneration while having the capability to bear appropriate amounts of load. To achieve this, the construct must allow sufficient nutrient infiltration to sustain cell recruitment, differentiation, and tissue remodeling after implantation. The scaffold must also provide adequate strength to support surrounding tissue and new tissue during development. It is well accepted that

such requirements can be achieved using porous scaffolds as the basis of the tissue-engineered construct; however, there is no data that identify how permeable these constructs must be to support or enhance bone regeneration. In this work, permeability effects on bone growth *in vivo* were determined with scaffolds of low and high ( $5.8 \times$  low) permeability.

The utilization of SFF techniques allows more rigorous control of scaffold architecture compared to previous studies where salt leached,<sup>18</sup> gas foamed, or emulsion constructs demonstrated that higher porosity enhances osteogenesis.<sup>22,23</sup> For this work, pore size (1 mm), pore shape (spherical), and pore interconnectivity (100%) were kept constant between the two permeability designs (high and low). Variation in permeability was created through changing the amount of overlap between spherical pores, which resulted in differences in porosity, throat size, and surface area, as these design features are interrelated. Higher porosity often results in higher scaffold surface area, which enhances ion exchange and bone-inducing factor adsorption, provided that the scaffold material is hydrophilic and cell-friendly. However, increased porosity does not necessarily result in increased surface area, as demonstrated by the higher porosity scaffolds utilized in this work that had lower

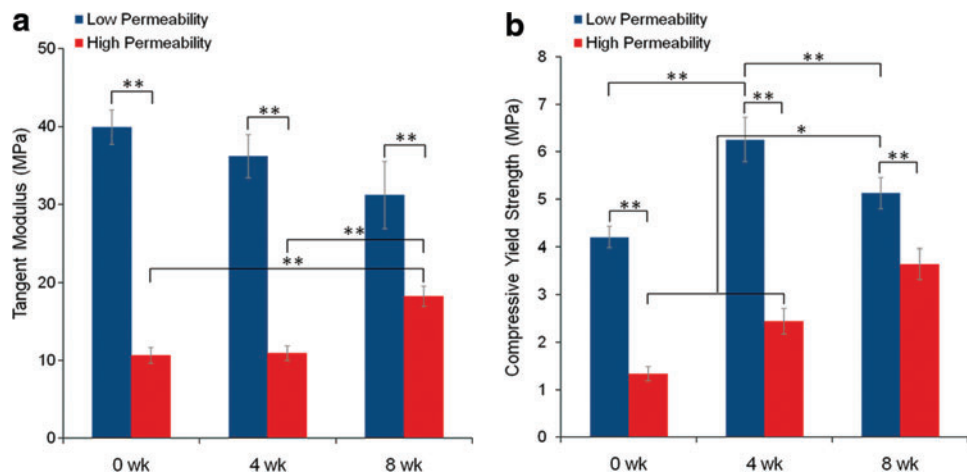


**FIG. 6.** (a) Tangent modulus at 12.5% strain, 4 and 8 weeks. (b) Compressive yield strength at 0.2% offset.  $*p \leq 0.05$ .  $**p \leq 0.01$ . Color images available online at [www.liebertonline.com/tea](http://www.liebertonline.com/tea)

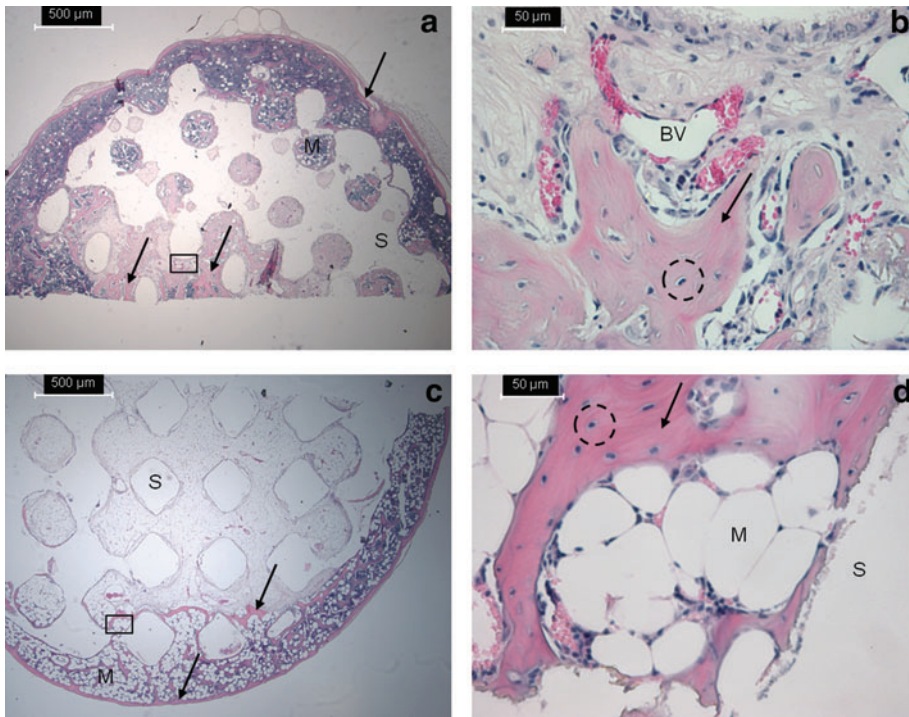


**FIG. 7.** Representative histological sections of high permeability (a, b) and low permeability (c, d) scaffolds at 8 weeks. (b) and (d) are higher magnification images of rectangular insets indicated in (a) and (c). The scaffold is indicated by "S" and bone growth in and around the scaffold is indicated by the dark pink staining and arrows. Osteocytes in lacunae are seen in both high and low permeability scaffolds (indicated by dashed circles) as is marrow space ("M"). Blood vessels are also seen in the high permeability scaffold (BV). Color images available online at [www.liebertonline.com/tea](http://www.liebertonline.com/tea)

surface area than the lower porosity scaffolds. It is possible that this decreased surface area may have been advantageous for cell infiltration due to the hydrophobicity of the PCL scaffold material used here.

Numerous studies (described below) demonstrate that pore size, interconnectivity, and porosity affect bone tissue regeneration, and these three design features appear to be the most important structural variables in an initial scaffold screening algorithm developed by Cleyenbreugel *et al.*<sup>22</sup> for bone tissue engineering applications. It is difficult to keep all three of these variables constant and create two scaffolds of differing permeability that can be built successfully. The scaffolds used here were successfully designed to hold two out of the three variables constant, pore size and interconnectivity, to elucidate changes in bone growth caused only by variations in permeability. Pore and throat size, mutually and collectively, influence the diffusion of materials through a scaffold and thus affect nutrient delivery and cell infiltration. Gross pore size alone influences the mode of bone tissue development. A minimum pore size of 300  $\mu\text{m}$  is required for microvessel formation, which greatly improves the flow of nutrients to the interior of the scaffold.<sup>24</sup> Larger pores (>300  $\mu\text{m}$ ) lead to direct osteogenesis as opposed to endochondral ossification. Jones *et al.*<sup>2</sup> argue that accessible pore size is the most relevant design variable to consider for bone infiltration into a scaffold, and that it must be at least 100  $\mu\text{m}$ . Scaffolds used in this work were designed with a pore size of 1000  $\mu\text{m}$ , allowing ample space for cells and vessels to infiltrate and bone tissue to develop. The larger pore size also enabled manufacturing of regular pore architecture by SFF. However, large pore size does not guarantee successful tissue regeneration since the overall pore architecture affects accessibility of internal scaffold pores. Throat size and accessible pore size, together, enable initial cell penetration and nutrient and waste diffusion. Otsuki *et al.*<sup>25</sup>

found that 52  $\mu\text{m}$  is the minimum throat size allowable for adequate bone and tissue in-growth *in vivo*.  $\mu\text{CT}$  quantification and histology in this work illustrate the effectiveness of larger throat sizes (390 and 610  $\mu\text{m}$  for the low and high permeability designs, respectively), as bone penetrated into the center of both scaffold design groups.

There have been few studies that directly examined construct permeability and its effect on bone regeneration. Hui *et al.*<sup>26</sup> proposed that below a threshold fluid conductance, vascularization into cancellous autograft constructs was poor and bone regeneration minimal. However, when interpreting fluid conductance (permeability times construct area divided by construct length) data, it is unclear whether the intrinsic permeability is limiting bone in-growth or whether the size of the construct requires a longer time for creeping substitution of bone. Jones *et al.*<sup>2</sup> proposed that the fluid conductance data of Hui *et al.*<sup>26</sup> along with their own data suggest a minimum intrinsic permeability of  $3 \times 10^{-8} \text{ m}^4/\text{Ns}$  to allow bone in-growth independent of the time period. The permeabilities of scaffolds used in this study were 6.9 and  $39.9 \times 10^{-8} \text{ m}^4/\text{Ns}$ , well above the threshold permeability proposed by Jones *et al.*<sup>2</sup> To further examine how the scaffold designs used here affected the growth of bone into interior void spaces, percent increases in scaffold BV from 4 to 8 weeks were calculated for each scaffold design group. The high permeability scaffolds showed an average increase in scaffold BV of 106%, whereas low permeability scaffolds had only a 62.3% increase. Granted, these average values do not account for variability, but they suggest that, in this model, increasing permeability may increase the rate and penetration of bone in-growth into the interior void spaces of scaffolds. Advantageous to tissue engineering applications that employ such findings, the variable of permeability is not confined by a particular pore size or shape to achieve desired properties, enabling optimization of mechanical properties

or other tissue regeneration constraints in light of permeability requirements.

It has been postulated that scaffolds for bone regeneration should have a minimum compressive strength of 2 MPa and a minimum modulus of 50 MPa, which are at the low range of properties for trabecular bone. Strength values reported here for both scaffold designs are well within this suggested value. Moduli for the low permeability scaffolds reached 50 MPa, whereas those of the high permeability design did not. This is not particularly concerning though, since the 50 MPa modulus value refers to mature bone, and the scaffold will primarily be supporting immature, developing bone. The results suggest that the modulus of the high permeability scaffold/tissue construct will continue to increase as more bone penetrates the void space and becomes mineralized. It would be prudent to also evaluate stiffer materials for their ability to regenerate bone successfully, but with any material, a tradeoff exists between mechanical properties and diffusion characteristics, as discussed below.

There is a balance that must be met between increasing mass transport characteristics (in this case permeability) and providing adequate scaffold mechanical properties, both of which are dependent on scaffold internal architecture and material. For a given material, increasing permeability requires increasing void space in the scaffold, thereby decreasing mechanical properties. Expectedly, the two PCL scaffold designs (low and high permeability) utilized in this work resulted in two different mechanical property profiles. Low permeability scaffolds had a significantly higher ( $p \leq 0.01$ ) average modulus than high permeability scaffolds. This trend endured through the eighth week of *in vivo* implantation, suggesting that the greater amount of PCL scaffold material in these scaffolds was still supporting most of the mechanically applied load during testing. For the high permeability design there was a significant increase ( $p \leq 0.05$ ) in mechanical properties at 8 weeks, which is evident for both modulus and compressive yield strength. This suggests that for this scaffold design, the bone in-growth and penetration into the inside of the scaffold at 8 weeks is contributing to the mechanical strength and beginning to bear more load than the PCL scaffold itself. High permeability scaffolds exhibited an increasing modulus trend from 4 to 8 weeks, which can be explained by the 117% increase in TMC from 4 to 8 weeks for this design. This mature bone is capable of bearing significant amounts of load during compressive testing and appears to have a large influence on the mechanical properties of the bone-PCL construct. This phenomenon was not observed for the low permeability design, which may be due to the lesser degree of bone in-growth and scaffold degradation due to the presence of thicker struts. This suggests that a high permeability scaffold design may be beneficial not only for enhancing new bone growth as compared to less permeable designs, but also for providing adequate mechanical properties to support this developing tissue and surrounding tissues at the implantation site.

## Conclusions

In this study, scaffolds were created with rigorously controlled architectures designed to specifically study the influence of permeability on bone regeneration. Results presented here show that higher permeability scaffolds support greater amounts of bone in-growth in a model that

utilizes BMP-7-transduced HGFs seeded into PCL scaffolds and implanted in nude mice for up to 8 weeks. Bone in-growth in high permeability scaffolds, in turn, increased the mechanical properties of these PCL-bone constructs from 0 to 8 weeks. Future studies may include (1) longer time *in vivo* to examine the effect of PCL degradation on construct fidelity and to better understand the balance of tissue in-growth and scaffold degradation over time, (2) expansion of permeability ranges evaluated, and (3) testing of size-appropriate constructs in the orthotopic sites of large animals. From the analyses presented here, we conclude that a more permeable scaffold environment is more favorable for bone growth using PCL scaffolds in our *in vivo* mouse model.

## Acknowledgments

The authors would like to thank Eiji Saito for his assistance with animal surgeries and Colleen Flanagan for her assistance with  $\mu$ CT. This work was funded by NIH RO1 AR 053379.

## Disclosure Statement

The authors confirm that there are no known conflicts of interest associated with this article and there has been no significant financial support for this work that could have influenced its outcome.

## References

1. Karande, T.S., Ong, J.L., and Agrawal, C.M. Diffusion in musculoskeletal tissue engineering scaffolds: design issues related to porosity, permeability, and nutrient mixing. *Ann Biomed Eng* **32**, 1728, 2004.
2. Jones, A.C., Arns, C.H., Huttmacher, D.W., Milthorpe, B.K., Sheppard, A.P., and Knackstedt, M.A. The correlation of pore morphology, interconnectivity and physical properties of 3D ceramic scaffolds with bone ingrowth. *Biomaterials* **30**, 1440, 2009.
3. Lee, K.E., Wang, S., Fox, B.C., Ritman, E.L., Yaszemski, M.J., and Lu, L. Poly(propylene fumarate) bone tissue engineering scaffold fabrication using stereolithography: effects of resin formulations and laser parameters. *Biomacromolecules* **8**, 1077, 2007.
4. Wang, K., Cai, L., Hao, F., Xu, X., Cui, M., and Wang, S. Distinct cell responses to substrates consisting of poly- $\epsilon$ -caprolactone and poly(propylene fumarate) in the presence or absence of cross-links. *Biomacromolecules* **11**, 2748, 2010.
5. Ciapetti, G., Ambrosio, L., Savarino, L., Granchi, D., Cenni, E., Baldini, N., *et al.* Osteoblast growth and function in porous poly- $\epsilon$ -caprolactone matrices for bone repair: a preliminary study. *Biomaterials* **24**, 3815, 2003.
6. Williams, J.M., Adewumni, A., Schek, R.M., Flanagan, C.L., Krebsbach, P.H., Feinberg, S.E., *et al.* Bone tissue engineering use polycaprolactone scaffolds fabricated via selective laser sintering. *Biomaterials* **26**, 4817, 2005.
7. Roosa, S.M.M., Kempainen, J.M., Moffit, E.N., Krebsbach, P.H., and Hollister, S.J. The pore size of polycaprolactone scaffolds has limited influence on bone regeneration in an *in vivo* model. *J Biomed Mater Res A* **92A**, 359, 2009.
8. Yamoso-Scholl, K., Jacobson, J.A., Bradica, G., Lerner, A.L., O'Keefe, R.J., Schwarz, E.M., Zuscik, M.J., and Awad, H.A. Evaluation of dense polylactic acid/beta-tricalcium phosphate scaffolds for bone tissue engineering. *J Biomed Mater Res A* **95**, 717, 2010.



9. Tanaka, Y., Yamaoka, H., Nishizawa, S., Nagata, S., Ogasawara, T., Asawa, Y., Fujihara, Y., Takato, T., and Hoshi, K. The optimization of porous polymeric scaffolds for chondrocyte/atelocollagen based tissue-engineered cartilage. *Biomaterials* **31**, 4506, 2010.
10. Mooney, D.J., Baldwin, D.F., Suh, N.P., Vacanti, J.P., and Langer, R. Novel approach to fabricate porous sponges of poly(D,L-lactic-co-glycolic acid) without the use of organic solvents. *Biomaterials* **17**, 1417, 1996.
11. Saito, E., Kang, H., Taboas, J.M., Diggs, A., Flanagan, C.L., and Hollister, S.J. Experimental and computational characterization of designed and fabricated 50:50 PLGA porous scaffolds for human trabecular bone applications. *J Mater Sci Mater Med* **21**, 2371, 2010.
12. Hollister, S.J., Lin, C.Y., Saito, E., Schek, R.D., Taboas, J.M., Williams, J.M., Partee, B., Flanagan, C.L., Diggs, A., Wilke, E.N., Van Lenthe, G.H., Muller, R., Wirtz, T., Das, S., Feinberg, S.E., and Krebsbach, P.H. Engineering craniofacial scaffolds. *Orthod Craniofac Res* **8**, 162, 2005.
13. Wilson, C.E., van Blitterswijk, C.A., Verbout, A.J., Dhert, W.J., and de Bruijn, J.D. Scaffolds with a standardized macro-architecture fabricated from several calcium phosphate ceramics using an indirect rapid prototyping technique. *J Mater Sci Mater Med* **22**, 97, 2011.
14. Sugawara, A., Fujikawa, K., Hirayama, S., Takagi, S., and Chow, L.C. *In vivo* characteristics of premixed calcium phosphate cements when implanted in subcutaneous tissues and periodontal bone defects. *J Res Natl Inst Stand Technol* **115**, 277, 2010.
15. Zein, I., Hutmacher, D.W., Tan, K.C., and Teoh, S.H. Fused deposition modeling of novel scaffold architectures for tissue engineering applications. *Biomaterials* **23**, 1169, 2002.
16. Kweon, H.Y., Yoo, M.K., Park, I.K., Kim, T.H., Lee, H.C., Lee, H.-S., *et al.* A novel degradable polycaprolactone network for tissue engineering. *Biomaterials* **24**, 801, 2003.
17. Krebsbach, P.H., Gu, K., Franceschi, R.T., and Rutherford, R.B. Gene therapy-directed osteogenesis: BMP-7-transduced human fibroblasts form bone *in vivo*. *Hum Gene Ther* **11**, 1201, 2000.
18. Suh, S.W., Shin, J.Y., Kim, J., Kim, J., Beak, C.H., Kim, D.I., *et al.* Effect of different particles on cell proliferation in polymer scaffolds using a solvent-casting and particulate leaching technique. *ASAIO J* **48**, 460, 2002.
19. Schek, R.M., Wilke, E.N., Hollister, S.J., and Krebsbach, P.H. Combined use of designed scaffolds and adenoviral gene therapy for skeletal tissue engineering. *Biomaterials* **27**, 1160, 2006.
20. Kempainen, J.M., and Hollister, S.J. Differential effects of designed scaffold permeability on chondrogenesis by chondrocytes and bone marrow stromal cells. *Biomaterials* **31**, 279, 2010.
21. Chen, Q., Kaji, H., Iu, M.F., Nomura, R., Sowa, H., Yamauchi, M., *et al.* Effects of an excess and a deficiency of endogenous parathyroid hormone on volumetric bone mineral density and bone geometry determined by peripheral quantitative computed tomography in female subjects. *J Clin Endocrinol Metab* **88**, 4655, 2003.
22. Cleyenbreugel, T.V., Schrooten, J., Oosterwyck, H.V., and Sloten, J.V. Micro-CT-based screening of biomechanical and structural properties of bone tissue engineering scaffolds. *Med Biol Eng Comput* **44**, 517, 2006.
23. Karageorgiou, V., and Kaplan, D. Porosity of 3D biomaterial scaffolds and osteogenesis. *Biomaterials* **26**, 5474, 2005.
24. Van Tienen, T.G., Heijkants, R.G.J.C., Buma, P., de Groot, J.H., Pennings, A.J., and Veth, R.P.H. Tissue ingrowth and degradation of two biodegradable porous polymers with different porosities and pore sizes. *Biomaterials* **23**, 1731, 2002.
25. Otsuki, B., Takemoto, M., Fujibayashi, S., Neo, M., Kokubo, T., and Nakamura, T. Pore throat size and connectivity determine bone and tissue ingrowth into porous implants: three-dimensional micro-CT-based structural analyses of porous bioactive titanium implants. *Biomaterials* **27**, 5892, 2006.
26. Hui, P.W., Leung, P.C., and Sher, A. Fluid conductance of cancellous bone graft as a predictor for graft-host interface healing. *J Biomech* **29**, 123, 1996.

Address correspondence to:

Scott J. Hollister, Ph.D.

Departments of Biomedical Engineering

University of Michigan

Lurie Biomedical Engineering Building

Room 2208, 1101 Beal Ave.

Ann Arbor, MI 48109

E-mail: scottho@umich.edu

Received: September 22, 2010

Accepted: March 10, 2011

Online Publication Date: April 25, 2011

